processes

MDPI

Article

Diagnosis of Multiple Short-Circuit Faults in Three-Phase Induction Motors Using Electric Phasor Analysis of Line Currents and Fuzzy Logic

Josue A. Reyes-Malanche [1,†], Efrain Ramirez-Velasco [2,†], Francisco J. Villalobos-Pina [2,*,†] and Eduardo-Cabal Yepez [3,†]

[1] Departamento de Produccion y Seguridad Industrial, Universidad Tecnologica de Aguascalientes, Aguascalientes 20200, Mexico; josue.malanche@utags.edu.mx
[2] Departamento de Ingeniería Electrica Electronica, TecNm/Instituto Tecnologico de Aguascalientes, Aguascalientes 20256, Mexico; r21153203@aguascalientes.tecnm.mx
[3] Multidisciplinary Studies Department, Engineering Division, University of Guanajuato, Campus Irapuato-Salamanca, Guanajuato 38944, Mexico; e.cabalyepez@gmail.com
* Correspondence: francisco.vp@aguascalientes.tecnm.mx
† These authors contributed equally to this work.

Abstract: The three-phase induction motor (IM) plays an essential role in industry; therefore, ensuring these motors operate under faultless and reliable conditions. Previous studies have reported that 28% to 38% of IM failures are related to the stator windings. For this reason, numerous efforts have been made to develop low-cost procedures for early fault detection in IMs. However, their primary drawback is that they involve complex mathematical operations for analyzing acquired information in the frequency or time-frequency domains, making online implementation challenging. Consequently, there remains a need for a reliable, online method to detect faulty conditions in IMs. In this work, a straightforward methodology based on the phasor-representation analysis and a fuzzy logic classifier is proposed for the online detection and classification of short-circuit faults in a three-phase IM. The signal-processing technique in this approach involves basic arithmetic operations, making it feasible for implementation on the Texas Instruments 32-bit, floating-point digital signal processor TMS320F28335. The obtained results demonstrate the efficacy and utility of the proposed methodology in detecting and classifying incipient or simultaneous short-circuit faults. It significantly reduces processing time while achieving high precision and accuracy compared to previous approaches reported in recent literature.

Keywords: phasor analysis; short-circuit; multiple faults; induction motor; fuzzy logic

check for updates

Academic Editors: Gloria Lilia Osorio-Gordillo and Marouane Alma

Received: 9 November 2024
Revised: 13 December 2024
Accepted: 27 December 2024
Published: 31 December 2024

Citation: Reyes-Malanche, J.A.; Ramirez-Velasco, E.; Villalobos-Pina, F.J.; Yepez, E.-C. Diagnosis of Multiple Short-Circuit Faults in Three-Phase Induction Motors Using Electric Phasor Analysis of Line Currents and Fuzzy Logic. *Processes* **2025**, *13*, 70. https://doi.org/10.3390/pr13010070

Copyright: © 2024 by the authors. Licensee MDPI, Basel, Switzerland. This article is an open access article distributed under the terms and conditions of the Creative Commons Attribution (CC BY) license (https://creativecommons.org/licenses/by/4.0/).

1. Introduction

The induction motor (IM) plays an important role in industry due to its advantages over other electric rotating machines. Hence, there is a strong demand for this type of motor to operate under faultless and reliable conditions since, otherwise, there would be stoppages generating significant losses in profits and maintenance [1]. Previous studies have described how, in an IM, 44% of faults are associated with bearing damages and 8% with rotor defects; 28% to 38% of IM failures are related to stator windings, and around 22% are related to other types of failures [2]. For the diagnosis of faults in three-phase induction electric machines, there are various techniques, including techniques based on signal processing, such as the discrete Fourier transform (DFT), wavelet transform, short-time Fourier transform (STFT), multiple signal classifier, Hilbert–Huang transform, etc. [3];

techniques based on data handling, such as artificial neural networks (ANNs), fuzzy logic, genetic algorithms, etc. [3]; and techniques based on mathematical models [4]. Therefore, considerable efforts have been made in the development of low-cost procedures for early detection of IM faults, which can avoid machine degradation. New supervision schemes are characterized as being online and noninvasive, with the capability of detecting faults while the machine is operating [5].

Nowadays, online monitoring of IMs is becoming increasingly important; however, the lack of a reliable method to recognize a faulty condition in IMs still presents a challenge. Hence, distinct approaches have been proposed to tackle this issue. For instance, in [6], the authors used the magnitude of phase currents and a fuzzy system to detect electrical short-circuit faults between IM coils. In [7], an approach is utilized to detect faults in the stator of rotating IMs; unfortunately, as the magnitude of phase currents varies depending on motor load levels, implementing a relatively large database is necessary to detect faults through a fuzzy logic system. A different approach involves analyzing stator currents using the Teager–Kaiser energy operator before performing their spectral analysis [8]. This method can effectively remove the main component of the electric current using minimal computer resources by utilizing three consecutive samples from the current supply signal. The Teager–Kaiser energy operator can increase the signal–noise ratio during the spectral analysis, refining the frequency peaks that show the presence of a faulty condition; however, some cases have shown that the occurrence of a fault is often accompanied by complex physical phenomena that affect other spectral components [9]. In a different approach, faults among the coils of an IM were analyzed [10]. Multiple reference frameworks were used, and an eccentricity indicator, also known as the instantaneous space-phasor Park module (ISP), was applied to enhance the Park approach in a modified 3-hp, squirrel-cage motor to establish distinct levels of fault severity.

A non-invasive method [11], which used the analysis of electric currents during the transient and steady states along with the analysis of infrared data captured through thermal cameras, was presented for detecting electromechanical faults in an IM; each of these methodologies provides complementary information that can be useful for diagnosing a wide range of faults. A diagnostic technique [12] based on acoustic signals from faultless cases, as well as bearing faults and combined bearing and winding faults in motors, was presented for early fault detection. This method analyzes the current signal from a single phase in the IM and utilizes the selection of amplitudes of frequency multi-expanded (MSAF-20-MULTIEXPANDED) for feature extraction. Another technique for detecting electrical faults was performed by measuring the external magnetic field of an IM. This technique is based on the discrete wavelet transform energy computation during the transient condition, where the machine operates at startup and standstill states. The wavelet transform offers a fine analysis of unidimensional and two-dimensional signals; thus, it is possible to extract information for the prognosis of different faulty conditions utilizing a multilevel discrete wavelet decomposition. The stored energy calculation from each decomposition evaluates the fault severity, in comparison to the analysis of the external magnetic field only [13]. Incipient short-circuit faults in electric machines powered by inverters are detected using discrete wavelet transform, a statistical parameter from detail and approximate coefficients of various decomposition levels, and a support vector machine (SVM) [14]. Multiple faults are detected [15] through a dynamic mathematical model of a permanent magnet synchronous motor based on structural analysis. The diagnosis system implements a generalized likelihood ratio test algorithm to detect coil inter-turn short circuits and encoder faults. The use of compensation for negative sequence current was proposed [16], where incipient faulty conditions in an IM were isolated. The main drawback of all these techniques involves their reliance on methodologies involving

intricate procedures and complex mathematical operations. These operations analyze the acquired information in the frequency or time-frequency domains using various artificial intelligence (AI) schemes.

This work proposes a straightforward methodology based on a phasor-representation analysis and a fuzzy logic classifier that utilizes the Mamdani inference rule and the centroid defuzzification method for detecting and isolating short-circuit faults in the three-phase IM. The proposed scheme only requires three Hall effect sensors; the benefit of using this type of sensor is significant, as it allows for non-invasive data acquisition while being cost-effective. Commercially, low-cost Hall effect sensors are available to acquire the stator line currents of IM for monitoring purposes. Phase currents are estimated from these line currents, enabling analysis using two different algorithms designed to discriminate between short circuits in one winding or two windings, respectively. Based on experimental results, the proposed approach has been demonstrated to accurately identify both incipient and severe electrical short-circuit faults simultaneously in one or two windings of an IM.

The document is structured as follows: Section 2 introduces the phasor analysis for detecting short-circuit faults in an IM. Section 3 describes the experimental setup used to assess the proposed technique. Section 4 shows the results of detecting incipient and severe faults in an IM. Finally, Sections 5 and 6 provide the discussion and conclusions, respectively, regarding the introduced technique.

2. Stator Winding Fault Analysis

Stator electrical faults are analyzed through the following phasor relationships between line (1) and phase (2) currents of the induction motor stator. These line current and phase current relationships, considering the induction motor in normal operation, are depicted in Figure 1 with per unit magnitudes.

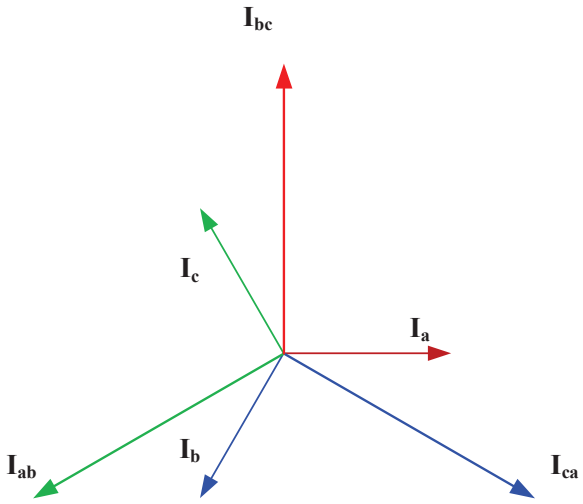


Figure 1. Phase current and line current phasor representations.

Phasor representation of the acquired stator line currents (1) and phase currents (2); this approach was validated only for star configuration.

$$\begin{aligned} I_{bc} &= \sqrt{3}\angle 90^\circ \\ I_{ca} &= \sqrt{3}\angle -30^\circ \\ I_{ab} &= \sqrt{3}\angle -150^\circ \end{aligned} \tag{1}$$

$$\begin{aligned} I_a &= 1\angle 0^\circ = (\mathbf{I}_{ca} - \mathbf{I}_{ab})/3 \\ I_b &= 1\angle -120^\circ = (\mathbf{I}_{ab} - \mathbf{I}_{bc})/3 \\ I_c &= 1\angle 120^\circ = (\mathbf{I}_{bc} - \mathbf{I}_{ca})/3 \end{aligned} \tag{2}$$

In an electrically balanced three-phase system connected to an induction motor, due to the absence of a neutral-line connection, the stator supply currents meet the following conditions in star or delta configurations, due to the absence of the neutral line.

$$\mathbf{I}_a + \mathbf{I}_b + \mathbf{I}_c = 0 \tag{3}$$

It is possible to obtain phasor components or coordinates for each current in relation to the different reference systems; from Figure 1 (1), (2), it can be seen that a specific phase current is always perpendicular to a corresponding line current as described below:

$$\begin{array}{ccc} \mathbf{I}_{bc} & \perp & \mathbf{I}_a \\ \mathbf{I}_{ca} & \perp & \mathbf{I}_b \\ \mathbf{I}_{ab} & \perp & \mathbf{I}_c \end{array} \tag{4}$$

Figure 2 depicts how each phasor can be represented by its corresponding components along the reference framework built through $\mathbf{I}_{bc}$ and $\mathbf{I}_a$ ($\mathbf{I}_{bc} \perp \mathbf{I}_a$), generating the line and phase current expressions in (5).

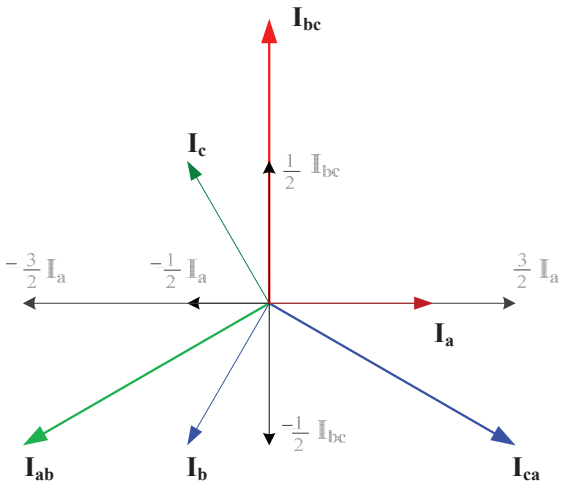


Figure 2. Current phasor components along the reference framework $\mathbf{I}_{bc} \perp \mathbf{I}_a$.

$$\begin{array}{rcl} \mathbf{I}_{ab} & = & \frac{1}{2}(-3\mathbf{I}_a - \mathbf{I}_{bc}) \\ \mathbf{I}_{ca} & = & \frac{1}{2}(3\mathbf{I}_a - \mathbf{I}_{bc}) \\ \mathbf{I}_{bc} & = & \mathbf{I}_{bc} \\ \mathbf{I}_a & = & \mathbf{I}_a \\ \mathbf{I}_b & = & \frac{1}{2}(-\mathbf{I}_a - \mathbf{I}_{bc}) \\ \mathbf{I}_c & = & \frac{1}{2}(-\mathbf{I}_a + \mathbf{I}_{bc}) \end{array} \tag{5}$$

Considering the previous approach, equivalent expressions, such as those in (5), can be obtained for the reference frameworks $\mathbf{I}_{ca} \perp \mathbf{I}_b$ and $\mathbf{I}_{ab} \perp \mathbf{I}_c$.

2.1. *Single Short-Circuit Fault Diagnosis*

Phasor representations facilitate the development of a diagnostic scheme to detect magnitude and phase-angle fluctuations in these currents when a single coil fault occurs. Figure 3 presents the trajectory changes on the phasors when a fault appears in $\mathbf{I}_{bc}$.

When the line current phasor $\mathbf{I}_{bc}$ increases due to a fault in the corresponding stator winding, the remaining phase- and line current phasors shift parallel to the line current in a faulty condition but in the opposite direction, as depicted in Figure 4. The direction and magnitude changes of the phasors are computed utilizing the expressions in (5). Since

the fault on line current $\mathbf{I}_{bc}$ is represented upward, the shifts in the line currents $\mathbf{I}_{ca}$ and $\mathbf{I}_{ab}$ go down. It is noteworthy that the phase current $\mathbf{I}_a$ neither changes its magnitude nor its phase angle, whereas the magnitude and phase angle of $\mathbf{I}_b$ and $\mathbf{I}_c$ change. The described behavior of the phasors, when a single fault occurs, is obtained as a result of choosing the reference framework $\mathbf{I}_{bc} \perp \mathbf{I}_a$, which contains the faulty line current phasor $\mathbf{I}_{bc}$. Therefore, the behavior must be considered for diagnosing single faults. The faulty condition can be detected and isolated by observing the phase current that remains unchanged. In Figure 4, the magnitude and angle variations of line and phase current phasors (black lines), when there is a faulty condition on $\mathbf{I}_{bc}$, are depicted. Since just the phase current $\mathbf{I}_a$ remains unaltered, it means that the line current $\mathbf{I}_{bc}$ is under a faulty condition, increasing its magnitude, which allows detecting and isolating the short-circuit single failure.

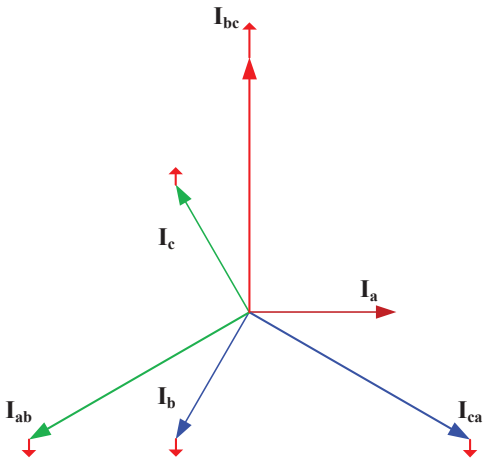


Figure 3. The variation in the direction of the current phasor due to a single fault on $\mathbf{I}_{bc}$.

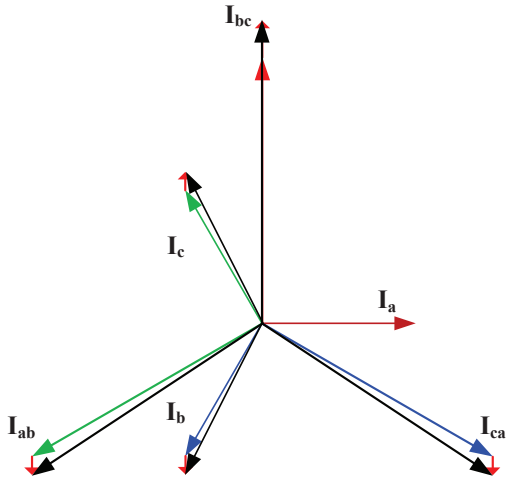


Figure 4. Current phasor shifting with a single fault on $\mathbf{I}_{bc}$.

2.2. Double Short-Circuit Fault Diagnosis

Equivalent expressions to those shown in (5) must be considered for determining magnitude and angle variations of line and phase current phasors under a double electrical fault. Figure 5 shows the phasor direction changes generated by each faulty condition on line currents $\mathbf{I}_{bc}$ and $\mathbf{I}_{ca}$, considering reference frameworks $\mathbf{I}_{bc} \perp \mathbf{I}_a$, and $\mathbf{I}_{ca} \perp \mathbf{I}_b$.

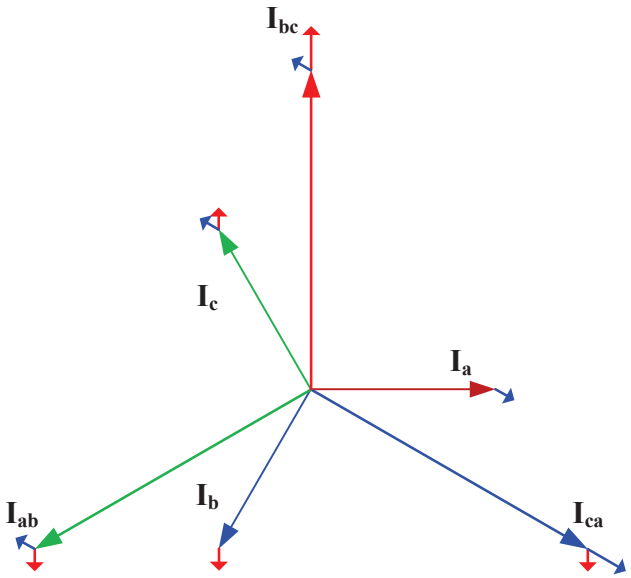


Figure 5. Current-phasor variations and directional changes associated with a double fault on the stator windings.

Figure 6 shows the magnitude and direction variations (black lines) of current phasors when a double fault develops. It can be observed that the largest current-phasor fluctuations develop in the direction of the faulty line currents, that is, in the direction of line currents $\mathbf{I}_{bc}$ and $\mathbf{I}_{ca}$, whereas the remaining current phasor variations are minimal. For instance, the phase current $\mathbf{I}_a$ changes its direction toward the line current $\mathbf{I}_{ca}$, whereas the trajectory of the phase current phasor $\mathbf{I}_b$ is adjusted in the opposite direction of the line current phasor $\mathbf{I}_{bc}$.

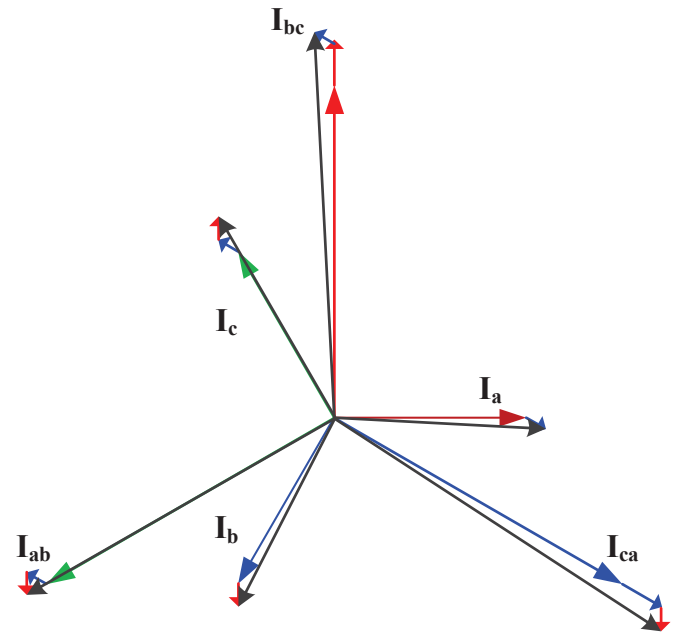


Figure 6. The shifting of current phasors with a double fault on $\mathbf{I}_{bc}$ and $\mathbf{I}_{ca}$.

The sum of vector variations for each current phasor represents the resultant variation due to the double fault. This can be diagnosed by analyzing the phase current phasor, which exhibits two significant variations, as depicted in Figure 5 for the phase current $\mathbf{I}_c$. The faulty condition is identified, considering the phase current phasor $\mathbf{I}_c$, which is directly related to the line currents $\mathbf{I}_{bc}$ and $\mathbf{I}_{ca}$ under failure, showing a higher magnitude than the other phase current phasors $\mathbf{I}_a$ and $\mathbf{I}_b$.

3. Experimental Setup

An experimental test bench was developed, composed of a 3 hp, SIEMENS IM with a dual-star connection at 60 Hz, 220 V. Figure 7 depicts the proposed experimental scheme. The motor windings were altered to artificially induce the electrical faults, as shown in Figure 8. A three-phase full-bridge inverter was designed and developed based on the Mitsubishi Electric Corporation's CMD200DY-12H module. It can operate up to 600 V and 200 A. The power inverter executes a volts/hertz algorithm embedded in the DSP processor, which uses a 9 kHz carrier. For this reason, the current waves are clean, and the current signals are pure, without the need for any kind of signal processing. The only noise signal present in the current patterns is due to the high-frequency carrier, which is eliminated by the anti-aliasing filter included in the signal acquisition system. This filter has a cutoff frequency of 600 Hz, and the bandwidth of the frequencies of interest ranges between 0 and 200 Hz, so the noise associated with the carrier does not pose any problem. Only a low-pass anti-aliasing filter with a cutoff frequency of 500 Hz is used at the DSP input processor for each channel. A data acquisition, power electronics driver control, and computational tool have been developed using the Texas Instruments TMS320F28335, a 32-bit floating-point digital signal processor. The designed system can modify the sampling frequency, ensuring the quality of fault diagnosis is maintained as long as the chosen sampling frequency complies with the Nyquist sampling theorem. It executes a real-time current signal acquisition and examination algorithm developed in Delphi 7 visual language. This system allows for variation in the data acquisition sampling frequency and the amount of information gathered in each experiment. Figure 9 depicts the developed test bench.

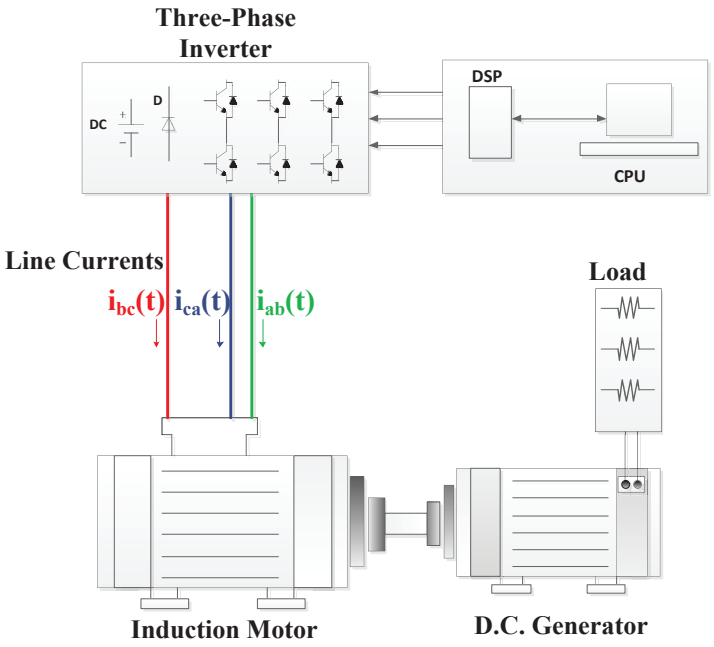


Figure 7. Schematic of the test bench.

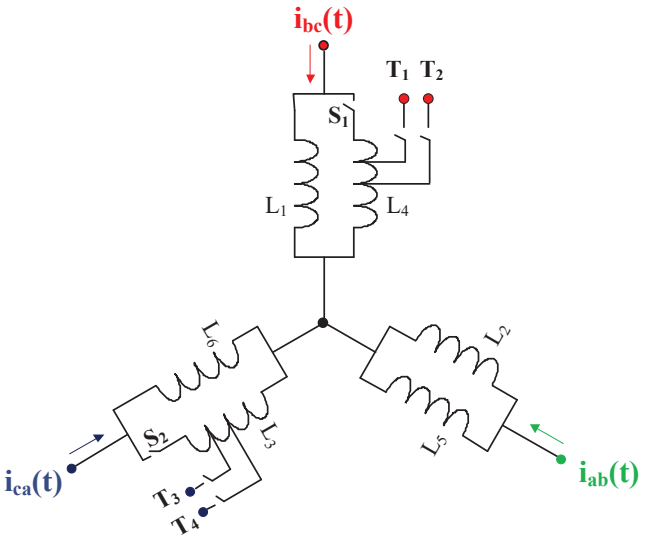


Figure 8. Double-star winding configuration in an induction motor stator.

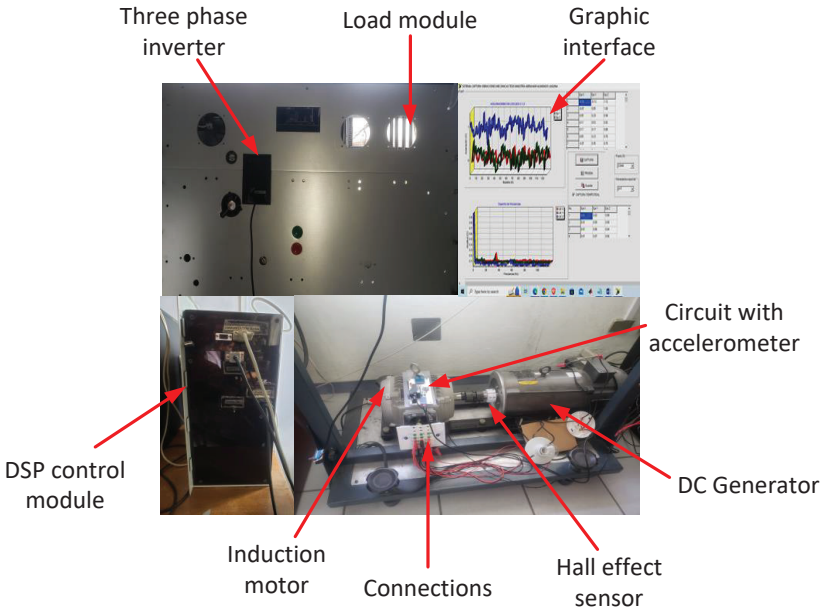


Figure 9. Test bench details.

Fuzzy Logic Fault Diagnosis Algorithm

Fuzzy logic is a redundant tool that enables the validation of phasorial analysis using three simple rules in each case to detect and isolate the short-circuit faults in one or two windings of the induction motor stator. Two different Mamdani-based fuzzy logic algorithms were implemented—one for the case of a single faulty winding and the other for two faulty windings simultaneously—using the corresponding Matlab toolbox. These algorithms are designed for detecting and isolating a single short-circuit fault or a simultaneous double fault in the induction motor windings. Figure 10 describes the fuzzy logic-based procedure for identifying line and phase current asymmetries to classify the faults in the stator coils.

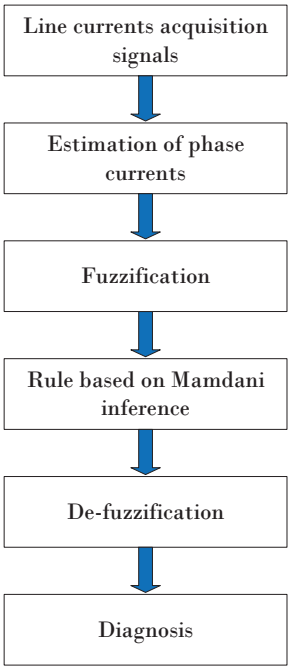


Figure 10. Fuzzy-logic classification of faults based on Mamdani inference.

A set of fuzzy rules is produced to detect and isolate faults. Tables 1 and 2 describe these classification rules for the single and simultaneous faults, respectively.

Table 1. Set of fuzzy rules for detecting a single fault corresponding to $\mathbf{I}_{bc}$.

Number	Rule
1	If $\mathbf{I}_a$, $\mathbf{I}_b$, $\mathbf{I}_c$, $\mathbf{I}_{ab}$, $\mathbf{I}_{ca}$ and $\mathbf{I}_{bc}$ are faultless then faultless motor
2	If $\mathbf{I}_a$, $\mathbf{I}_b$, $\mathbf{I}_c$, $\mathbf{I}_{ab}$, $\mathbf{I}_{ca}$ and $\mathbf{I}_{bc}$ are incipient then fault in $\mathbf{I}_{bc}$
3	If $\mathbf{I}_a$, $\mathbf{I}_b$, $\mathbf{I}_c$, $\mathbf{I}_{ab}$, $\mathbf{I}_{ca}$ and $\mathbf{I}_{bc}$ are drastic then fault in $\mathbf{I}_{bc}$

Table 2. Set of fuzzy rules for identifying a simultaneous double fault corresponding to $\mathbf{I}_{bc}$ and $\mathbf{I}_{ca}$.

Number	Rule
1	If $\mathbf{I}_a$, $\mathbf{I}_b$, $\mathbf{I}_c$, $\mathbf{I}_{ab}$, $\mathbf{I}_{ca}$, $\mathbf{I}_{bc}$ are faultless then faultless motor
2	If $\mathbf{I}_a$, $\mathbf{I}_b$, $\mathbf{I}_c$, $\mathbf{I}_{ab}$, $\mathbf{I}_{ca}$, $\mathbf{I}_{bc}$ are incipient then fault in $\mathbf{I}_{bc}$ and $\mathbf{I}_{ca}$
3	If $\mathbf{I}_a$, $\mathbf{I}_b$, $\mathbf{I}_c$, $\mathbf{I}_{ab}$, $\mathbf{I}_{ca}$, $\mathbf{I}_{bc}$ are drastic then fault in $\mathbf{I}_{bc}$ and $\mathbf{I}_{ca}$

Figure 11 shows the fuzzy system for detecting and isolating a faulty condition on the stator winding corresponding to $\mathbf{I}_{bc}$, which depicts the three possible scenarios: faultless condition, incipient, and severe fault. In this figure, it can be observed that the magnitude of the phase current $\mathbf{I}_a$ remains unaffected; however, $\mathbf{I}_{bc}$ shifts right, as it can be deduced from (5), meaning its magnitude increases because of the fault.

A similar procedure to that shown in Figure 11, must be followed to detect and isolate two short-circuit faults occurring simultaneously in two different windings. But in this case, the phase current that must be considered for the analysis is the one whose direction changes twice ($\mathbf{I}_c$), following the description in the methodology and illustrated in Figure 5.

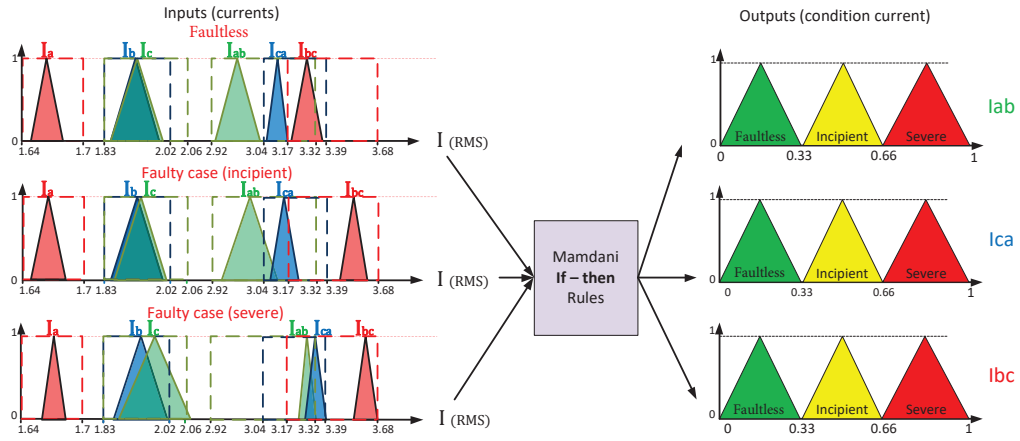


Figure 11. Fuzzy system for detecting and isolating a single fault corresponding to $\mathbf{I}_{bc}$.

4. Experimental Results

The analyzed signals were obtained experimentally from a test bench, which included an induction motor customized to artificially induce short-circuit faults in its stator windings, as depicted in Figure 8. The ordinary resistance and inductance values for the employed induction motor in faultless condition are shown in Table 3.

Table 3. Common resistance and inductance values for the utilized induction motor in the faultless condition.

Coils	Terminals	R (Ω)	Inductance (mH)
L1	1, 4	4.25	53.12
L2	7, 10	4.39	54.92
L3	2, 5	3.07	38.35
L4	8, 11	4.21	52.61
L5	3, 6	3.59	44.85
L6	9, 12	3.71	46.35

From Table 3, it can be observed that there is an unbalance among the currents of the induction motor windings since they are different, which provokes a higher magnitude of the line current $\mathbf{I}_{bc}$ than those of $\mathbf{I}_{ab}$ and $\mathbf{I}_{ca}$; these line currents are obtained directly from the experimental test bench, whereas the values of phase currents $\mathbf{I}_a$, $\mathbf{I}_b$, and $\mathbf{I}_c$ must be computed by (5), as shown in Table 4.

Table 4. RMS values of the phase and line currents for an induction motor in a faultless condition.

Trial	$\mathbf{I}_a$	$\mathbf{I}_b$	$\mathbf{I}_c$	$\mathbf{I}_{ab}$	$\mathbf{I}_{ca}$	$\mathbf{I}_{bc}$
1	1.66	1.88	1.84	2.99	3.14	3.18
2	1.66	1.90	1.87	3.02	3.08	3.26
3	1.65	1.92	1.95	3.01	3.17	3.38
4	1.67	1.84	1.92	2.93	3.11	3.23
5	1.67	1.85	1.88	3.03	3.06	3.19

Each coil of the stator has 45 turns; Table 5 presents the short-circuited turns, resistance, inductance, and percentage values resulting from reducing the number of turns on each winding through the switches $\mathbf{T}_1$, $\mathbf{T}_2$, $\mathbf{T}_3$, and $\mathbf{T}_4$, as depicted in Figure 8. For each analyzed condition, 30 different trials were performed during experimentation.

Table 5. Resistance and inductance values obtained by inducing short-circuit faults on the induction motor windings through the switches T1, T2, T3, and T4.

Switch	Turns	R (Ω)	Inductance (mH)	Percent Per Coil
T1	5	3.67	45.85	11.11%
T2	12	3.08	38.47	26.66%
T3	7	2.59	33.55	14.00%
T4	17	1.91	24.72	37.77%

4.1. Single Short-Circuit Fault Detection and Isolation

The fuzzy logic algorithm receives the line and phase currents as inputs for detecting and isolating the faults. If the machine is in a faultless condition, the result from the fuzzy-logic algorithm will be 0.165 for all three windings, as displayed in Figure 12. From this figure, it can be observed that the output obtained by the centroid defuzzification method for the three line currents, $\mathbf{I}_{bc}$, $\mathbf{I}_{ab}$, and $\mathbf{I}_{ca}$, is 0.165. This means that the three corresponding windings are in faultless condition, according to the pre-established values for this status, which range from 0 to 0.33 on the universe of discourse from 0 to 1. Figure 13 shows the obtained line currents when the motor is in faultless condition; it is worth noting that the SIEMENS 3 hp motor is powered by a three-phase full-bridge inverter with 220 V AC.

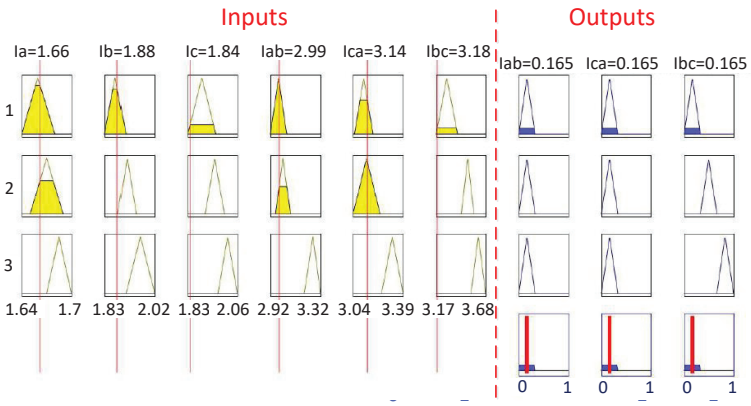


Figure 12. Defuzzification values for the faultless condition of the induction machine.

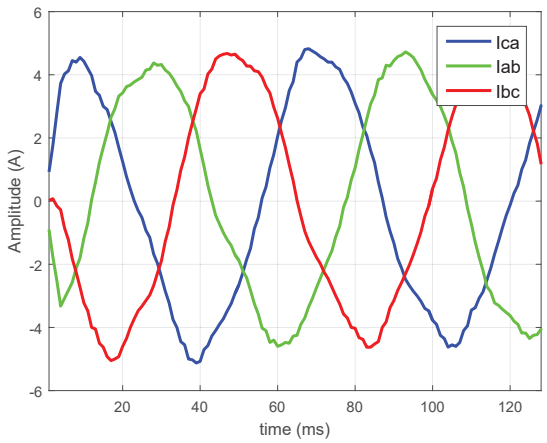


Figure 13. Line currents of an IM in the faultless case.

When a short-circuit occurs on the line current $\mathbf{I}_{bc}$, the winding fed by this line current is in a faulty condition. For instance, when switch $\mathbf{T}_3$ is activated, it generates a short-circuit on 7 turns of the L_3 winding. Switching on $\mathbf{T}_3$ increases the line current $\mathbf{I}_{bc}$, and

the magnitudes of the phase currents $\mathbf{I}_b$ and $\mathbf{I}_c$. So, the line currents $\mathbf{I}_{ab}$ and $\mathbf{I}_{ca}$ increase because of the short circuit condition, whereas the phase current $\mathbf{I}_a$ barely changes its magnitude, keeping it to the corresponding faultless condition value. This is depicted in Table 6, where the first column for $\mathbf{I}_a$ shows a mean value of 1.67, and line current $\mathbf{I}_{bc}$ increases in magnitude 3.48. In the faultless condition, the mean value of the phase current $\mathbf{I}_a$ is 1.66 and line current $\mathbf{I}_{bc}$ is 3.25. Figure 14 shows the line stator currents.

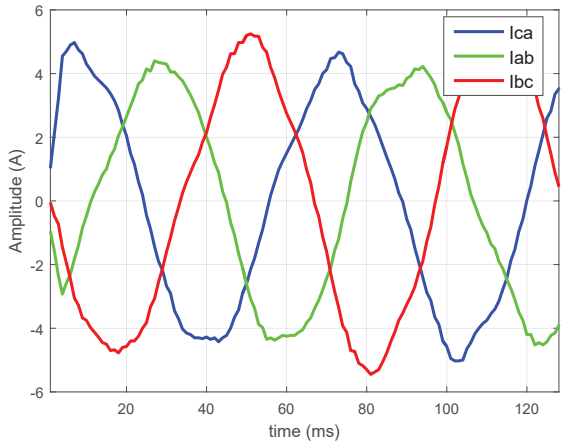


Figure 14. Line currents for 7 short-circuited turns in $\mathbf{I}_{bc}$.

Table 6. RMS values of phase and line currents for 7 short-circuited turns in $\mathbf{I}_{bc}$.

Trial	$\mathbf{I}_a$	$\mathbf{I}_b$	$\mathbf{I}_c$	$\mathbf{I}_{ab}$	$\mathbf{I}_{ca}$	$\mathbf{I}_{bc}$
1	1.68	1.95	1.98	3.05	3.14	3.54
2	1.67	1.92	1.98	3.03	3.17	3.51
3	1.66	1.89	1.95	2.97	3.11	3.45
4	1.67	1.94	1.92	3.07	3.05	3.47
5	1.68	1.90	1.96	3.06	3.21	3.44

Figure 15 shows the proposed system response when 7 turns are short-circuited. The line current $\mathbf{I}_{bc}$ value is around 0.495 according to the centroid defuzzification method. The pre-established span for detecting this condition goes from 0.33 to 0.66; whereas the $\mathbf{I}_{ab}$ and $\mathbf{I}_{ca}$ values are around 0.165 on the universe of discourse from 0 to 1, which implies they are in faultless condition. The fault isolation is performed by observing the increase in $\mathbf{I}_b$ and $\mathbf{I}_c$ magnitudes, whereas $\mathbf{I}_a$ remains at its faultless condition value.

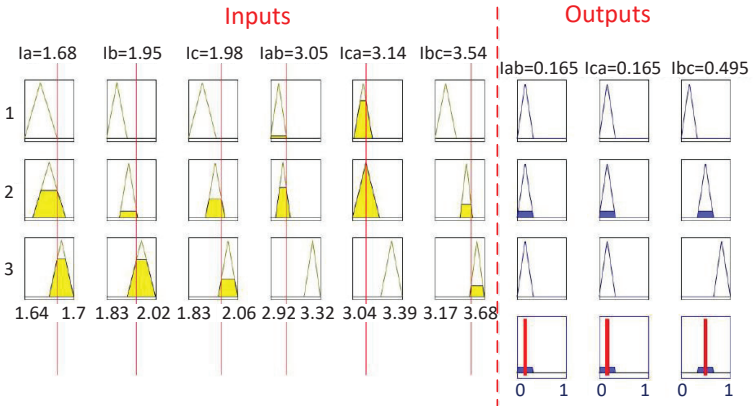


Figure 15. Defuzzification values for identifying 7 turns in fault corresponding to $\mathbf{I}_{bc}$.

Switching on $\mathbf{T}_4$ sets 17 turns in the short-circuit condition on the L_3 winding; hence, the magnitudes of line current $\mathbf{I}_{bc}$, and phase currents $\mathbf{I}_b$ and $\mathbf{I}_c$ further increase their values,

whereas $\mathbf{I}_a$ remains at its faultless condition value shown in Table 7, where the mean value of $\mathbf{I}_a$ is 1.68, close to 1.66, while the line current $\mathbf{I}_{bc}$ has a mean value of 3.62, higher than 3.25. Figure 16 illustrates the magnitude increments on line current $\mathbf{I}_{bc}$, and phase currents $\mathbf{I}_b$ and $\mathbf{I}_c$, as validated by the RMS values and obtained through the corresponding phasor analysis (see Table 7).

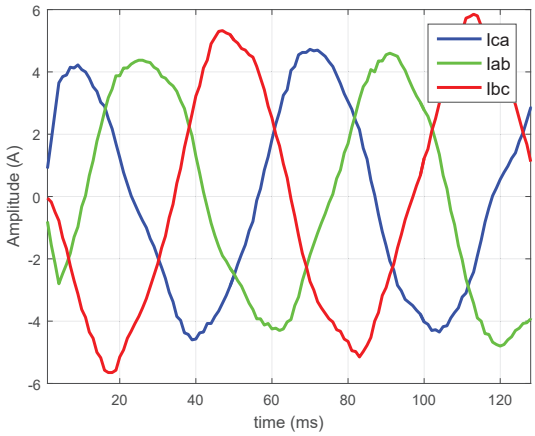


Figure 16. Line currents with 17 turns in the fault corresponding to $\mathbf{I}_{bc}$.

Table 7. RMS values of phase and line currents for 17 turns in fault in $\mathbf{I}_{bc}$.

Trial	$\mathbf{I}_a$	$\mathbf{I}_b$	$\mathbf{I}_c$	$\mathbf{I}_{ab}$	$\mathbf{I}_{ca}$	$\mathbf{I}_{bc}$
1	1.68	1.97	2.04	3.31	3.28	3.65
2	1.68	1.98	1.98	3.28	3.25	3.58
3	1.69	1.99	2.05	2.25	3.33	3.67
4	1.68	1.91	1.99	3.21	3.38	3.54
5	1.68	2.01	2.07	3.25	3.34	3.66

Figure 17 portrays the obtained results when the RMS values given in Table 7 are used as input to the proposed method for detecting and isolating faults. From this figure, it can be observed that the output value for the line current $\mathbf{I}_{bc}$ is 0.83, utilizing the centroid defuzzification method. The membership region for this imperfection has been pre-established from 0.66 to 1, whereas the other two line currents, $\mathbf{I}_{ab}$ and $\mathbf{I}_{ca}$, stay at 0.165 since their corresponding windings are in faultless condition.

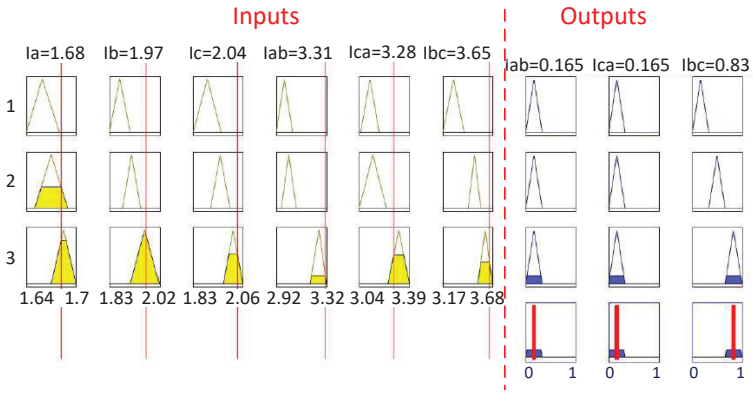


Figure 17. Defuzzification values for identifying 17 turns in the fault corresponding to $\mathbf{I}_{bc}$.

4.2. Double Short-Circuit Fault Detection and Isolation

To induce a double short-circuit fault, the switch $\mathbf{T}_1$ in the winding L_4, which corresponds to the line current $\mathbf{I}_{ca}$, is turned on for setting 5 turns in a short-circuit condition,

while the switch $\mathbf{T}_3$ in the winding L_3, which is associated with the line current $\mathbf{I}_{bc}$, is activated simultaneously to set 7 turns in a short-circuit condition. Table 8 shows the obtained RMS values for 5 out of 30 trials performed considering this condition. These values reveal the induced asymmetries on line and phase currents when a double fault occurs simultaneously in different windings for 5 and 7 turns. In this case, phase current $\mathbf{I}_c$ is the current that changes twice, as observed in Figures 5 and 6 with a mean value of 2.06. This is higher than the mean value of $\mathbf{I}_c$ of 1.89 from Table 4, which is the characteristic that allows isolating the two windings in fault corresponding to $\mathbf{I}_{bc}$ and $\mathbf{I}_{ca}$. The presence of a double fault in the same winding would imply a change in its impedance, resulting in an increase in the current. To achieve isolation of this type of fault, additional considerations would need to be taken into account.

Table 8. RMS values of phase and line currents for 5 and 7 simultaneously short-circuited coils in two different windings corresponding to $\mathbf{I}_{ca}$ and $\mathbf{I}_{bc}$.

Trial	$\mathbf{I}_a$	$\mathbf{I}_b$	$\mathbf{I}_c$	$\mathbf{I}_{ab}$	$\mathbf{I}_{ca}$	$\mathbf{I}_{bc}$
1	1.80	1.94	2.07	3.09	3.35	3.59
2	1.85	1.95	2.07	3.15	3.41	3.58
3	1.81	1.95	2.00	3.15	3.27	3.51
4	1.84	1.94	2.06	3.15	3.39	3.56
5	1.81	1.96	2.09	3.13	3.40	3.63

Figure 18 depicts the line currents for 5 and 7 simultaneously short-circuited turns in the two different windings corresponding to $\mathbf{I}_{ca}$ and $\mathbf{I}_{bc}$. In this figure, it can be observed that the $\mathbf{I}_{ca}$ and $\mathbf{I}_{bc}$ magnitudes increase compared to that of $\mathbf{I}_{ab}$, as reported in Table 8. On the other hand, the magnitudes of the phase currents $\mathbf{I}_a$, $\mathbf{I}_b$, and $\mathbf{I}_c$ increase too; however, the magnitude enlargement on one of the phase currents, $\mathbf{I}_c$, is noticeably higher than those of the two remaining ones, $\mathbf{I}_a$ and $\mathbf{I}_b$. This situation occurs because the phase current $\mathbf{I}_c$ is related to the two short-circuited windings corresponding to the line currents $\mathbf{I}_{ca}$ and $\mathbf{I}_{bc}$.

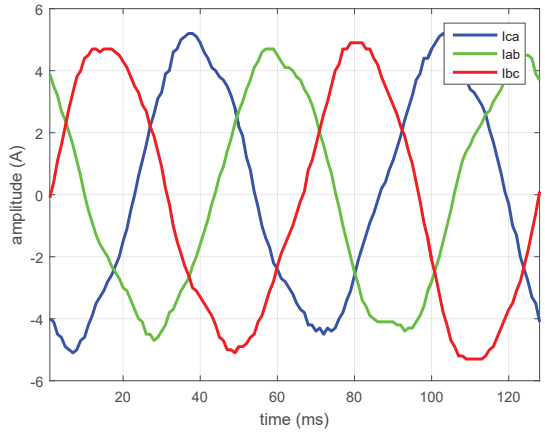


Figure 18. Line currents when a double fault occurs with 5 short-circuited turns corresponding to $\mathbf{I}_{ca}$ and 7 corresponding to $\mathbf{I}_{bc}$.

The RMS values obtained from this faulty scenario are used as input for the proposed approach. The outcomes for detecting and identifying double short-circuit faults are illustrated in Figure 19, where the association between the line currents $\mathbf{I}_{ca}$-$\mathbf{I}_{bc}$ shows an output value of 0.559. This indicates the presence of double short-circuit faults at their corresponding stator windings, which significantly increases the magnitude of the phase current $\mathbf{I}_c$ compared to those of phase currents $\mathbf{I}_a$ and $\mathbf{I}_b$, as shown in Table 8.

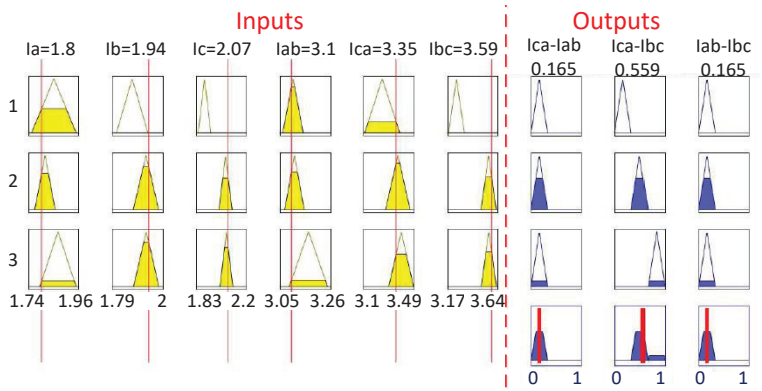


Figure 19. Defuzzification values for isolating a double short-circuit fault with 5 and 7 affected turns in two different windings corresponding to $\mathbf{I}_{ca}$ and $\mathbf{I}_{bc}$.

The second scenario for the double short-circuit fault involves the activation of switches $\mathbf{T}_2$ and $\mathbf{T}_4$ for exacerbating the faulty conditions from 5 and 7 to 12 and 17 short-circuited turns in $\mathbf{I}_{ca}$ and $\mathbf{I}_{bc}$, respectively. The obtained RMS values for the phase and line currents under this condition are reported in Table 9. In this case, phase current $\mathbf{I}_c$ is the current that changes twice, as observed in Figures 5 and 6, with a mean value of 2.07 that is higher than the mean value of $\mathbf{I}_c$ of 1.89 from Table 4, which is the characteristic that allows isolating the two windings in fault corresponding to $\mathbf{I}_{bc}$ and $\mathbf{I}_{ca}$. The corresponding waveforms are drawn in Figure 20, showing the asymmetric behaviors among them. It can be observed that $\mathbf{I}_{ca}$ and $\mathbf{I}_{bc}$ increase their values; consequently, $\mathbf{I}_c$ grows over the $\mathbf{I}_a$ and $\mathbf{I}_b$ amplitudes.

Table 9. RMS values of phase and line currents for 12 and 17 simultaneously short-circuited turns in the $\mathbf{I}_{ca}$ and $\mathbf{I}_{bc}$ corresponding windings.

Trial	$\mathbf{I}_a$	$\mathbf{I}_b$	$\mathbf{I}_c$	$\mathbf{I}_{ab}$	$\mathbf{I}_{ca}$	$\mathbf{I}_{bc}$
1	1.80	1.94	2.08	3.11	3.38	3.59
2	1.82	1.95	2.08	3.16	3.44	3.58
3	1.91	1.95	2.01	3.16	3.30	3.52
4	1.88	1.95	2.06	3.17	3.41	3.56
5	1.91	1.97	2.10	3.14	3.42	3.63

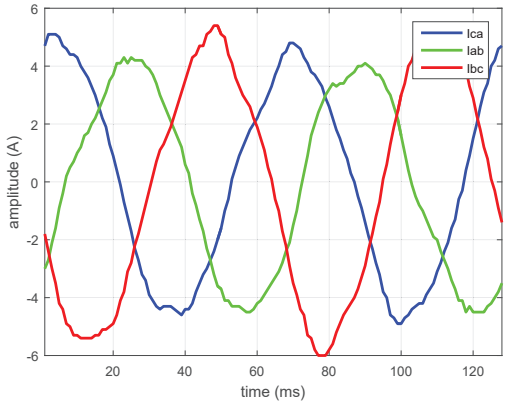


Figure 20. Line currents when a double fault occurs with 12 short-circuited turns corresponding to $\mathbf{I}_{ca}$ and 17 corresponding to $\mathbf{I}_{bc}$.

The proposed fuzzy-logic approach receives as inputs the RMS values of phase and line currents to detect and isolate the fault. The obtained results are illustrated in Figure 21,

where a significantly higher value of 0.83 can be noticed on the $\mathbf{I}_{ca}$-$\mathbf{I}_{bc}$ grouping, obtained through the centroid defuzzification method, which corresponds to the faulty stator windings.

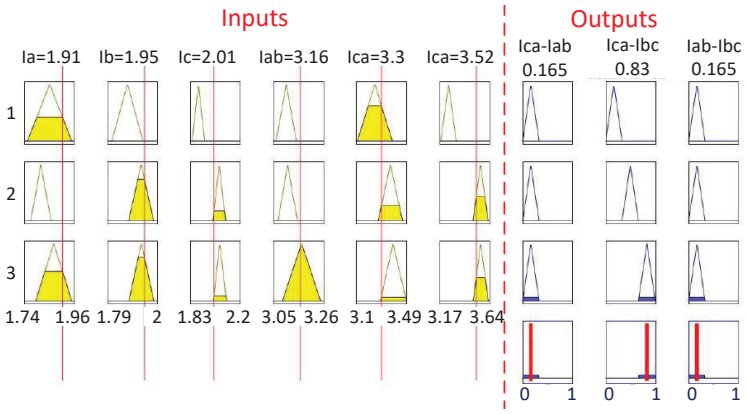


Figure 21. Defuzzification values for identifying a double short-circuit fault with 12 and 17 damaged coils in the $\mathbf{I}_{ca}$ and $\mathbf{I}_{bc}$ corresponding windings.

5. Discussion

The obtained results demonstrate that the proposed phasor analysis can be directly applied to electric current signals in the time domain, significantly reducing computational cost and processing time. This is because only basic arithmetic operations are needed to detect and discriminate among short-circuit faults, unlike previous approaches reviewed in the literature that require transforming the acquired signal from the time domain into the frequency domain for fault detection. Table 10 compares preceding approaches with the proposed technique in terms of computational cost, the ability to detect and classify short-circuit faults, and the processing time required to achieve an outcome. For further research, another type of electrical fault analysis will be validated. A limitation of this methodology is the simultaneous occurrence of power electronics drive and motor faults, which affect current magnitudes and make fault detection and isolation more challenging, similar to other methodologies.

Table 10. Comparison of the proposed method with other methods.

		Detection		Isolation		
Method	**Data**	**Single Fault**	**Double Fault**	**Single Fault**	**Simultaneous Double Fault**	**Execution Time**
AI [17,18]	6000, 30,000	Yes, Yes	No, No	No, No	No, No	156 s, 5 s
Model-based [19,20]	10,000, 200	Yes, Yes	No, No	Yes, No	No, No	1 s, >500 ms
Signal processing [21,22]	2500, 20,000	Yes, Yes	No, No	Yes, No	No, No	20.66 ms, >40 ms
Artificial vision [23]	1000	Yes	No	Yes	No	>200 ms
Proposed	128	Yes	Yes	Yes	Yes	40 ms

To demonstrate the accuracy rate of fault detection, a statistical analysis was performed. Figure 22 shows a normal distribution, revealing a slight unbalance in the stator currents caused by the manufacturing process. The mean value μ of a dataset under faultless conditions shows minimal normal variation.

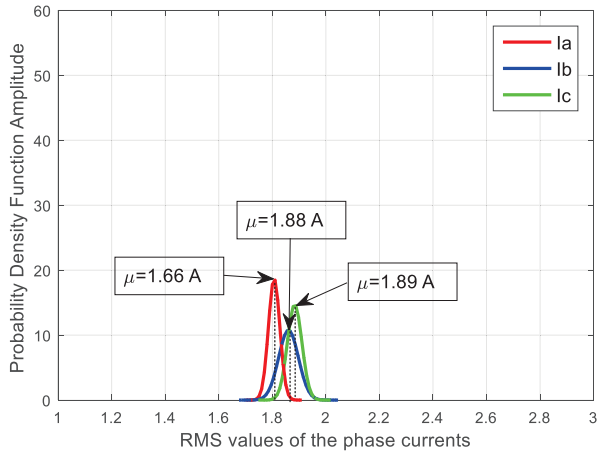


Figure 22. Normal distribution of line currents in the faultless scenario.

When the first fault scenario is generated by activating $\mathbf{T_3}$, currents $\mathbf{I}_b$ and $\mathbf{I}_c$ deviate further from current $\mathbf{I}_a$ due to the short-circuit of 7 turns in the winding corresponding to $\mathbf{I}_{bc}$, as illustrated in Figure 23. As observed in the figure, the current $\mathbf{I}_a$ has a μ value of 1.68 A, which is closer to $\mu = 1.66$ A from the faultless case (Figure 22). This, in conjunction with the phasorial analysis in Figure 3 from the methodology section, enables the isolation of the faulty winding.

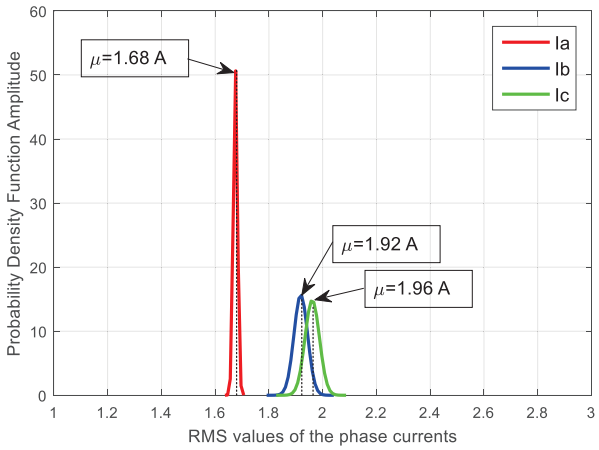


Figure 23. Normal distribution of line currents in a scenario with a 7-turn short-circuited fault scenario.

A second fault scenario is generated through $\mathbf{T_4}$. In this case, currents $\mathbf{I}_b$ and $\mathbf{I}_c$ increase their μ value regarding $\mathbf{I}_a$, where the value is 1.68 A close to 1.66 A from the faultless case shown in the phasorial analysis, although there is a short-circuit of 17 turns in the coil corresponding to $\mathbf{I}_{bc}$, which is illustrated in Figure 24, allowing to isolate the faulty winding.

The third scenario involves a double fault occurring simultaneously in different coils of the motor, with $\mathbf{T_1}$ and $\mathbf{T_3}$ generating a short-circuit fault of 5 and 7 turns in the windings corresponding to $\mathbf{I}_{ca}$ and $\mathbf{I}_{bc}$, respectively. The fourth scenario involves activating $\mathbf{T_2}$ and $\mathbf{T_4}$, generating short-circuit faults of 12 and 17 turns in the windings corresponding to $\mathbf{I}_{ca}$ and $\mathbf{I}_{bc}$ again. The normal distributions of the phase currents, as shown in Figures 25 and 26, present the phase current behaviors separating each other. This is due to the different magnitudes of $\mathbf{I}_{ab}$, $\mathbf{I}_{ca}$, and $\mathbf{I}_{bc}$, which affect the μ of $\mathbf{I}_a$, $\mathbf{I}_b$, and $\mathbf{I}_c$. As can be seen, current $\mathbf{I}_c$ is the most affected because two of the stator windings are in short-circuit faults at the

same time, specifically those supplying currents $\mathbf{I}_{ca}$ and $\mathbf{I}_{bc}$, as presented in Figures 5 and 6, which share current $\mathbf{I}_{c}$. It has also been observed that the normal distribution of $\mathbf{I}_{b}$ is narrower and taller than those of $\mathbf{I}_{a}$ and $\mathbf{I}_{c}$, as the variance in this current is significantly smaller compared to the other two.

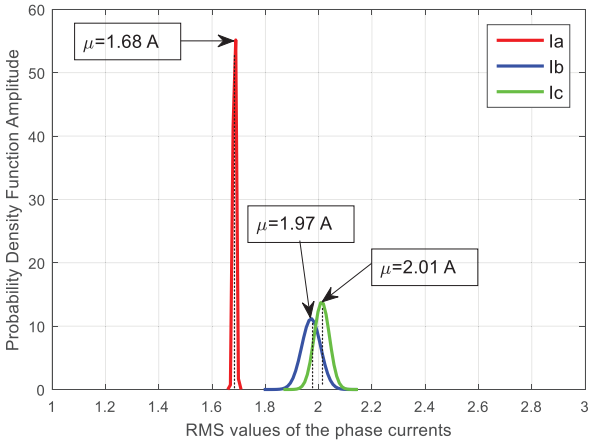


Figure 24. Normal distribution of line currents in a scenario with a 17-turn short-circuited fault scenario.

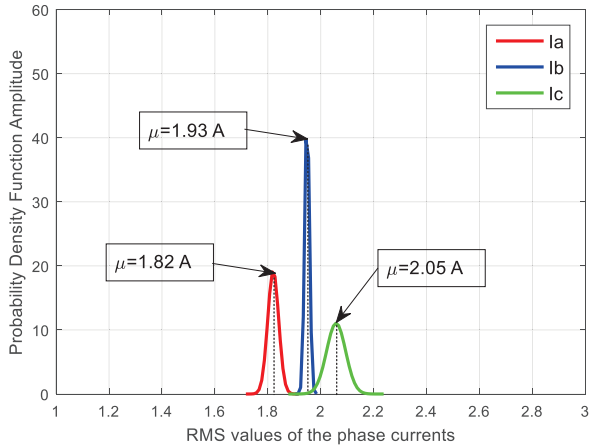


Figure 25. Normal distribution of line currents with the double-simultaneous short-circuit fault in the windings corresponding to 5 turns in $\mathbf{I}_{ca}$ and 7 turns in $\mathbf{I}_{bc}$.

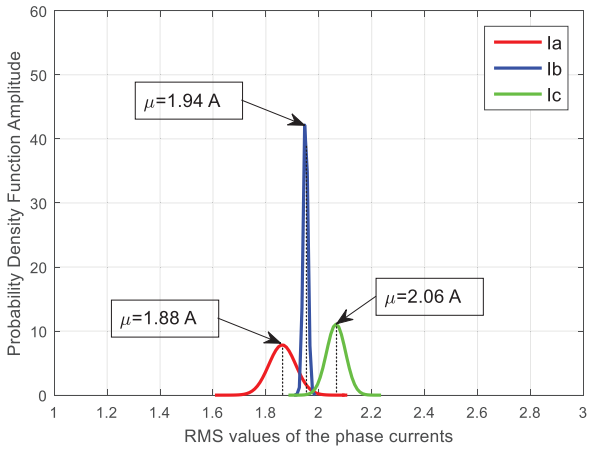


Figure 26. Normal distribution of line currents with a double-simultaneous short-circuit fault in the windings corresponding to 12 turns in $\mathbf{I}_{ca}$ and 17 turns in $\mathbf{I}_{bc}$.

6. Conclusions

In modern applications, it is essential to maintain induction motors (IM) in a faultless and reliable condition. Extensive studies have shown that 28% to 38% of IM failures are caused by defects in the stator windings; hence, several fault detection and classification procedures have been proposed and implemented. However, most of these rely on elaborate strategies involving complex mathematical operations to analyze acquired electric current and/or vibration signals in the frequency or time-frequency domains, making them extremely challenging to implement online. The merit of this work lies in the introduction of a technique that uses fundamental arithmetic operations for phasor computations. This approach is designed to detect and classify incipient and severe short-circuit faults through fuzzy logic. The proposed method analyzes phase and line currents in the steady state and in the time domain. Because of its low computational cost, it can be integrated into the TMS320F28335 digital signal processor, which allows real-time fault diagnosis. It is also possible to evaluate complex fault scenarios. The results obtained from 30 trials on a deliberately modified induction motor, designed to simulate distinct fault scenarios, have demonstrated the efficacy of the proposed method. The method performed online detection and classification of incipient and severe short-circuit faults in significantly less computation time than recently proposed approaches in the reviewed literature. The method detects faults only when a variation exceeds the imbalance threshold. Graphs were generated to observe current variations in the steady state, demonstrating that any variation outside the range of currents observed under faultless conditions would be detected. It is known that the phase current perpendicular to the line in a short circuit does not vary, as shown by the probability distribution functions. Future work might include the design and development of digital structures to perform the hardware implementation of the proposed methodology for incipient and severe faults in a field programmable gate array (FPGA), taking advantage of its simplicity.

Author Contributions: J.A.R.-M. and E.R.-V.: methodology, data analysis, and results interpretation; F.J.V.-P.: experimentation for data acquisition, programming, and computing analysis; E.-C.Y.: manuscript writing, document preparation, and results interpretation. All authors have read and agreed to the published version of the manuscript.

Funding: This research received no external funding.

Data Availability Statement: Data are unavailable due to privacy reasons.

Acknowledgments: This work was partially supported by Departamento de Produccion y Seguridad Industrial, Universidad Tecnologica de Aguascalientes, Aguascalientes, DEPI-ITA-TecNm (Departamento de posgrado e investigacion-Instituto Tecnologico de Aguascalientes/Tecnologico Nacional de Mexico, and Multidisciplinary Studies Department, Engineering Division, Campus Irapuato-Salamanca, University of Guanajuato and finally to the Consejo de Nacional de Humanidades Ciencias y Tecnologías CONAHCYT.

Conflicts of Interest: The authors declare no conflicts of interest.

Abbreviations

The following abbreviations are used in this manuscript:

ANN	artificial neural network
AI	artificial intelligence
EPRI	Electric Power Research Institute
IM	induction motor
IEEE	Institute of Electrical and Electronics Engineers
PV	photovoltaic

SMV	support vector machine
RMS	root mean square

References

1. Siddiqui, K.M.; Sahay, K.; Giri, V.K. Health monitoring and fault diagnosis in induction motor—A review. *Int. J. Adv. Res. Electriacal Electron. Instrum. Eng.* **2014**, *3*, 6549–6565; ISSN:2278–8875.
2. Jigyasu, R.; Mathew, L.; Sharma, A.; Chatterji, S.A. Review of Condition Monitoring and Fault Diagnosis Methods for Induction Motor. In Proceedings of the Second International Conference on Intelligent Computing and Control Systems (ICICCS), Madurai, India, 14–15 June 2018; Volume 1, pp. 1–6. [CrossRef]
3. Yakhni, M.F.; Cauet, S.; Sakout, A.; Assoum, H.; Etien, E.; Rambault, L.; El-Gohary, M. Variable speed induction motors' fault detection based on transient motor current signatures analysis: A review. *Mech. Syst. Signal Process.* **2023**, *184*, 109737. [CrossRef]
4. Jalayer, M.; Orsenigo, C.; Vercellis, C. Fault detection and diagnosis for rotating machinery: A model based on convolutional LSTM, Fast Fourier and continuous wavelet transforms. *Comput. Ind.* **2021**, *125*, 103378. [CrossRef]
5. Alsaedi, M.A. Fault diagnosis of three-phase induction motor: A review. *Optics* **2015**, *4*, 1–8. [CrossRef]
6. Azgomi, H.F.; Poshtan, J. Induction Motor Stator Fault Detection via Fuzzy Logic. In Proceedings of the 21st Iranian Conference on Electrical Engineering (ICEE), Mashhad, Iran, 14–16 May 2013; Volume 1, pp. 1–5. [CrossRef]
7. Zamarron A.; Rodriguez S. Diagnostico de fallas en el motor de induccion usando logica difusa. *Rev. Iberoamercana Cienc.* **2015**, *2*, 163–171. Available online: http://www.reibci.org/publicados/2015/marzo/0900113.pdf (accessed on 28 December 2024).
8. Pineda-Sanchez, M.; Puche-Panadero, R.; Riera-Guasp, M.; Perez-Cruz, J.; Roger-Folch, J.; Pons-Llinares, J.; Climente-Alarco, V.; Antonino-Daviu, J.A. Application of the Teager–Kaiser energy operator to the fault diagnosis of induction motors. *IEEE Trans. Energy Convers.* **2013**, *28*, 1036–1044. [CrossRef]
9. Zouzou, S.E.; Sahraoui, M.; Ghoggal, A.; Guedidi, S. Detection of inter-turn short-circuit and broken rotor bars in induction motors using the Partial Relative Indexes: Application on the MCSA. In Proceedings of the XIX International Conference on Electrical Machines—ICEM 2010, Rome, Italy, 6–8 September 2010; pp. 1–6. [CrossRef]
10. Paz-Parra, A.; Amaya-Enciso, M.C.; Olaya-Ochoa, J.; Palacios-Penaranda, J.A. Stator fault diagnosis on squirrel cage induction motors by ESA and EPVA. In Proceedings of the Workshop on Power Electronics and Power Quality Applications (PEPQA), Bogota, Colombia, 6–7 July 2013; pp. 1–6. [CrossRef]
11. Picazo-Rodenas, M.J.; Antonino-Daviu, J.; Climente-Alarcon, V.; Royo-Pastor, R.; Mota-Villar, A. Combination of noninvasive approaches for gener l assessment of induction motors. *IEEE Trans. Ind. Appl.* **2015**, *51*, 2172–2180. [CrossRef]
12. Glowacz, A.; Glowacz, W.; Glowacz, Z.; Kozik, J. Early fault diagnosis of bearing and stator faults of the single-phase induction motor using acoustic signals. *Measurement* **2018**, *113*, 1–9. [CrossRef]
13. Cherif, H.; Menacer, A.; Romary, R.; Pusca, R. Dispersion field analysis using discrete wavelet transform for inter-turn stator fault detection in induction motors. In Proceedings of the IEEE 11th International Symposium on Diagnostics for Electrical Machines, Power Electronics and Drives (SDEMPED), Tinos, Greece, 29 August–1 September 2017; pp. 104–109. [CrossRef]
14. Vinayak, B.A.; An, K.A.; Jagadan, G. Waveletbasedreal-time stator fault detection of inverter-fed induction motor. *IET Electr. Power Appl.* **2020**, *14*, 82–90. [CrossRef]
15. Hasan Ebrahimi, S.; Choux, M.; Huynh, V.K. Real-Time Detection of Incipient Inter-Turn Short Circuit and Sensor Faults in Permanent Magnet Synchronous Motor Drives Based on Generalized Likelihood Ratio Test and Structural Analysis. *Sensors* **2022**, *22*, 3407. [CrossRef] [PubMed]
16. Bouzid, M.B.K.; Champenois, G.; Tnani, S. Reliable Stator Fault Detection Based on the Induction Motor Negative Sequence Current Compensation. *Int. J. Electr. Power Energy Syst.* **2018**, *95*, 490–498. [CrossRef]
17. Shao, S.; Yan, R.; Lu, Y.; Wang, P.; Gao, R.X. DCNN-based multi-signal induction motor fault diagnosis. *IEEE Trans. Instrum. Meas.* **2019**, *69*, 2658–2669. [CrossRef]
18. Saucedo-Dorantes, J.J.; Jaen-Cuellar, A.Y.; Perez-Cruz, A.; Elvira-Ortiz, D.A. Detection of Inter-Turn Short Circuits in Induction Motors under the Start-Up Transient by Means of an Empirical Wavelet Transform and Self-Organizing Map. *Machines* **2023**, *11*, 958. [CrossRef]
19. Babu, A.C.; Seshadrinath, J. Stator Inter-turn Fault Modelling and Analysis on Induction Motor based on MCCM. In Proceedings of the International Conference on Sustainable Energy and Future Electric Transportation (SEFET), Hyderabad, India, 21–23 January 2021; pp. 1–6. [CrossRef]
20. Sahin, I.; Keysan, O. Model Predictive Controller Utilized as an Observer for Inter-Turn Short Circuit Detection in Induction Motors. *IEEE Trans. Energy Convers.* **2021**, *36*, 1449–1458. [CrossRef]
21. Hussein, A.M.; Obed, A.A.; Zubo, R.H.A.; Al-Yasir, Y.I.A.; Saleh, A.L.; Fadhel, H.; Sheikh-Akbari, A.; Mokryani, G.; Abd-Alhameed, R.A. Detection and Diagnosis of Stator and Rotor Electrical Faults for Three-Phase Induction Motor via Wavelet Energy Approach. *Electronics* **2022**, *11*, 1253. [CrossRef]

22. Cherif, H.; Maamir, M.; Chehaidia, S.E. Analysis for inter turn stator fault with load variation in Induction Motor. *Int. J. Energetica* **2023**, *18*, 12–18. Available online: https://www.ijeca.info/index.php/IJECA/article/view/215 (accessed on 28 December 2024).
23. Wei, L.; Rong, X.; Wang, H.; Yu, S.; Zhang, Y. Method for Identifying Stator and Rotor Faults of Induction Motors Based on Machine Vision. *Math. Probl. Eng.* **2021**, *2021*, 1–13. [CrossRef]

Disclaimer/Publisher's Note: The statements, opinions and data contained in all publications are solely those of the individual author(s) and contributor(s) and not of MDPI and/or the editor(s). MDPI and/or the editor(s) disclaim responsibility for any injury to people or property resulting from any ideas, methods, instructions or products referred to in the content.